Journal of Pharmaceutical and Biomedical Analysis 47 (2008) 738–745

Contents lists available at ScienceDirect

Journal of Pharmaceutical and Biomedical Analysis

journal homepage: www.elsevier.com/locate/jpba

Process characterization of powder blending by near-infrared spectroscopy: Blend end-points and beyond

Zhenqi Shi[a], Robert P. Cogdill[b], Steve M. Short[a], Carl A. Anderson[a,b,*]

[a] Graduate School of Pharmaceutical Sciences, Duquesne University, Pittsburgh, PA 15282, United States
[b] Duquesne University, Center for Pharmaceutical Technology, Pittsburgh, PA 15282, United States

ARTICLE INFO

Article history:
Received 1 October 2007
Received in revised form 12 February 2008
Accepted 6 March 2008
Available online 22 March 2008

Keywords:
Powder blending
Near-infrared spectroscopy
End-point
Blending variability
Design of experiments

ABSTRACT

The purpose of this paper is to utilize near-infrared (NIR) spectroscopy to characterize powder blending in-line. A multivariate model-based approach was used to determine end-point and variability at the end-point of blending processes. Two monitoring positions for NIR spectrometers were evaluated; one was located on the top of the Bin-blender and the other was on the rotation axis. A ternary powder mixture including acetaminophen (APAP, fine and coarse powder), lactose (LAC) and microcrystalline cellulose (MCC, Avicel 101 and 200) was used as a test system. A Plackett–Burman design of experiments (DOE) for different blending parameters and compositions was utilized to compare the robustness of end-point determination between the multivariate model-based algorithm and reference algorithms. The end-point determination algorithm, including root mean square from nominal value (RMSNV) and two-tailed Student's *t*-test, was developed based on PLS predicted concentrations of all three constituents. Mean and standard deviation of RMSNV after end-point were used to characterize blending variability at the end-point. The blending end-point and variability of two sensors were also compared. The multivariate model-based algorithm proved to be more robust on end-point determination compared to the reference algorithms. Blending behavior at the two sensor locations demonstrated a significant difference in terms of end-point and blending variability, indicating the advantage to employ process monitoring via NIR spectroscopy on more than one location on the Bin-blender.

© 2008 Elsevier B.V. All rights reserved.

1. Introduction

Near-infrared (NIR) spectroscopy is a fast, non-invasive technique that has been demonstrated useful for pharmaceutical analysis of powder mixtures, granules, roller compacts, tablets and capsules without sample preparation [1]. Both chemical and physical information contained in the spectrum can be extracted via multivariate modeling. Monitoring of blending homogeneity is an important application of NIR spectroscopy. While traditional blending analysis including thief sampling and UV method considers only the active ingredient in a blend. NIR analyses allow consideration of all blend constituents simultaneously. Since most pharmaceutical active ingredients and excipients have unique NIR absorption spectra, multivariate techniques are used to resolve NIR spectra to predict concentration variation of all mixture components.

The interface of near-infrared spectroscopy to the blending process has included methods such as analysis of off-lines samples collected from a blender, and on-line or in-line real-time monitoring of powder mixing [2]. Following the collection of blending spectra, various qualitative and quantitative blend monitoring metrics have been used. Qualitative spectral analysis approaches include dissimilarity [3], Euclidean distance [3], mean square difference [4], moving-window standard deviation (MVSD) [5–7], PCA [3,6,8], SIMPLISMA [3], SIMCA [6,9], bootstrap algorithms and Chi-square analysis [9,10]. These approaches are based on calculation of spectral variance or multi-dimensional spectrum distance between continuous spectra or between target spectra of "ideal mixture" and individual spectra collected during the blending process. Quantitative approaches require a calibration model (e.g. PLS) to capture the concentration variation during the blending process [11–17]. Compared to quantitative approaches, qualitative approaches require less data and are therefore more suitable for early process development stages. However, a quantitative model is able to express blending processes in terms of concentration variation, which is comparable to the standard criteria of current regulatory requirements. While it is frequently argued that the concentration variation is implicit in qualitative methods, the

* Corresponding author at: Graduate School of Pharmaceutical Sciences, Duquesne University, Pittsburgh, PA 15282, United States. Tel.: +1 412 396 1102; fax: +1 412 396 4660.
E-mail address: andersonca@duq.edu (C.A. Anderson).

0731-7085/$ – see front matter © 2008 Elsevier B.V. All rights reserved.
doi:10.1016/j.jpba.2008.03.013

expression of variation is explicit in quantitative methods due to the specificity of a calibration model for a particular concentration variation. So far few reports compare the two methods directly, particularly with respect to robustness. Thus, a robustness comparison was performed in the paper between the multivariate model-based approach and widely used qualitative algorithms, moving window standard deviation (MVSD). Additionally, when a multivariate model is established for a powder blending unit operation, maintenance of model performance is an important issue. Thus, the effects of model performances on its monitoring capacity also require investigation.

It is well established that instability of a homogenous mixture can cause demixing or segregation after an end-point is reached, which can further lead to the problem of content non-uniformity [18]. An ideal powder blending process should be optimized for both homogeneity at unit-dose scale and stability (smallest variability) after end-point is reached. While most blending investigations focus on end-point determination, blending stability after end-point is seldom studied. Therefore, monitoring powder blending in terms of both end-point and blending variability warrants investigation.

In an early blending study by Sekulic et al. [5], a single optic fiber was inserted into the rotation axis of a V-blender to on-line measure the spectral variation with respect to time. But questions were posed as to whether a single fiber-optic probe is sufficient to represent overall concentration variation within the blender. More recently, it has been reported that multiple spectral sampling points in a V-blender are essential for accurate and precise estimation of end-points [7]. Due to differences in blending mechanisms and efficiencies between Bin- and V-blenders, it is necessary to evaluate the relationship between NIR sensor positioning and end-point determination in Bin-blenders.

The aim of this paper is to use a high rate of spectra collection to monitor in-line powder blending based on two NIR sensors positioned at the top and rotational axis of a Bin-blender. Blending end-point was determined based on a multivariate model-based statistical analysis of concentration variation with time. A Plackett–Burman design of experiment was utilized to compare the robustness of end-point determination between the proposed algorithm and the widely employed end-point determination metrics. The effects of model performance on end-point determination were investigated by adjusting the number of principle components (PCs), the slope and bias of prediction. After end-point determination, blending variability was characterized. The relationship between the position of NIR sensors and their capacity to monitor blending end-point and variability was also explored.

2. Materials and methods

2.1. Material

A ternary powder mixture was used, including: lactose (Foremost Farm USA, Rothschild, WI), Avicel (PH 101 and 200, FMC Biopolymer, Mechanicsburg, PA) and acetaminophen fine (Mallinckrodt Inc., Raleigh, NC) and coarse powder (Rhodia Organique, Cedex, France). The reported median particle size for the above components can be found in Table 1. All powder materials were used as received.

2.2. Blending

A stainless-steel 5.5-L Bin-blender with cylindrical top and cone bottom (L.B. Bohle, Germany) was used for all blending studies. The dimensions of the blender were 30.48 cm (height) × 20.32 cm (diameter of the top). Powders were loaded into the blender in the following order: lactose (LAC) first, followed by microcrystalline cellulose (MCC) and acetaminophen (APAP). The actual loading amount for each component was listed in Table 1. The blender was filled with powders to 80% (v/v) of the working capacity as a common industrial practice [19].

The blending composition and process condition were generated using a Plackett–Burman design (Table 1). In total, five variables were in the design matrix, including: APAP concentration, ratio of MCC/LAC, blending speed, APAP type and MCC type, respectively. Each design point was performed in triplicate experiments. Adequate variance was generated by the design matrix to demonstrate not only the capability of NIR spectroscopy in monitoring a variety of blending processes, but also the robustness of end-point determination methods.

2.3. Near-infrared spectroscopy

An anti-reflection coated window (10BW20-30, Newport, Mountain View, CA) was mounted onto the side wall of the blender, pointing towards the rotational axis. An NIR spectrometer (NIR-128L-1.7T-USB, Control Development, South Bend, IN) connected with an optic fiber, referred to as the side sensor, was inserted through a Teflon probe guide in front of the anti-reflection coated window. The side sensor had 400-μm spot size and 6.25-nm step-size. Another NIR spectrometer with wireless data collection (BM-1000, Control Development, South Bend, IN), named the top sensor, was mounted onto the top of the blender, where a cylindrical sample probe head (about 25-mm circular sensing area) protruded 5.53 cm (length) × 8.20 cm (diameter) into the blender. The dimension of the sensor was 37.97 cm × 20.06 cm × 17.14 cm. The top sensor was characterized by 3.125-nm step-size. It was reported that depth of penetration of NIR radiation in pharmaceutical powder was about 500 μm [20]. If a cylinder interrogation volume was assumed as reported, the volumes were 0.063 mm^3 and 245.44 mm^3 for side and top sensor, respectively. Taking into account of density of powder mixture, the calculated sample sizes for both sensors were well below the maximum allowed sample mass by FDA about 0.3–3 g [21]. Since the blender was 80% filled, powder was constantly in front of both spectrometers and spectra were collected continuously without rejection. A schematic diagram of the instrument can be found in Fig. 1. In order to capture

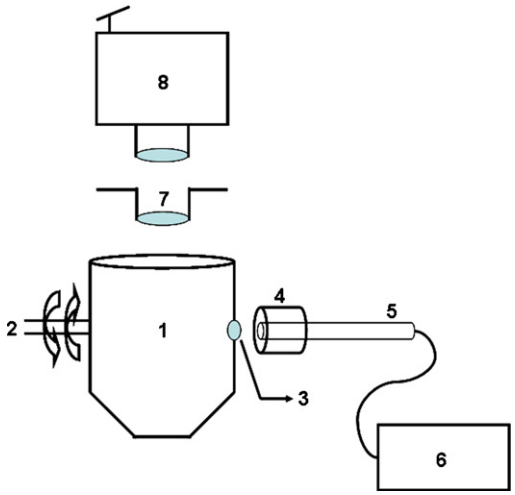

Fig. 1. Scheme of Bin-blender and two sensors. (1) Bin-blender; (2) rotation axis; (3) anti-reflection coated window; (4) Teflon probe guide; (5) fiber optics; (6) side sensor; (7) sample probe head; (8) top sensor.

Table 1
Plackett–Burman design matrix

Run #	APAP (w/w)	Ratio of MCC/LAC[a]	Blending speed (rpm)	APAP type[b]	MCC type[c]	Lactose (g)	MCC (g)	APAP (g)
1	0.15	2	25	Coarse powder	200	623.33	1246.67	330
2	0.05	2	15	Coarse powder	101	538.34	1076.66	85
3	0.15	0.5	15	Coarse powder	200	1382.67	691.33	366
4	0.05	0.5	25	Coarse powder	101	1329.99	665.01	105
5	0.15	2	25	Fine powder	101	470.33	940.67	249
6	0.05	2	15	Fine powder	200	646.01	1291.99	102
7	0.15	0.5	15	Fine powder	101	1110.67	555.33	294
8	0.05	0.5	25	Fine powder	200	1456.66	728.34	115

[a] The reported median particle size for lactose was 100 μm.
[b] The reported median particle size was 250 μm for APAP coarse powder and 100 μm for APAP fine powder.
[c] The reported median particle size was 180 μm for MCC PH200 and 50 μm for MCC PH101.

blending variability, spectra were collected at a rate of 5 s/spectra. This rate is significantly faster than the expected rate of change of the process; however, it is necessary to characterize the variability that changes on a time scale comparable to the stated collection rate. Each blending run was monitored for 90 min. The wavelength range was 911–1680 nm, with a 4-nm step size for a total of 193 variables.

In the above experimental setting, the probe head of the top sensor protruded into the Bin-blender due to the design of the sensor. While, certain disturbances could be expected, all blends were subjected to the same condition. Therefore, the robustness comparison among end-point determination algorithms and comparison between two sensors are reasonable.

2.4. Analysis of spectra

All spectral data were processed and analyzed in MATLAB (v7.1, The MathWorks, Natick, MA) using the PLS_Toolbox (v3.0, Eigenvector Research, Manson, WA) along with analysis routines developed in-house.

2.4.1. Comparison of end-point determination

Due to the better resolution, higher signal to noise ratio and larger interrogation volume of the top sensor, only data collected from top sensor were used for comparing robustness of end-point determination by different algorithms.

2.4.1.1. End-point determined by the multivariate model-based algorithm.

2.4.1.1.1. NIPLS calibration model. Non-linear iterative partial least square (NIPLS) was applied to establish a calibration model between the last 200 spectra of every blending run and corresponding nominal concentration of three components according to the design matrix. Because there were a total of 24 runs, the final spectral calibration data set (X) was 4800×193 and concentration data (Y) was 4800×3. Savitzky–Golay smoothing and derivative (window size = 15, 2nd polynomial order, 2nd derivative) and mean-centering were used as data pretreatments. Batch-wise cross validation was performed in order to select the optimal number of principle component. Batch was represented by one single blending run. After model calibration, concentrations of three components of each spectrum were predicted and the concentration–time profile for each blending experiment was plotted. Based on principle component analysis, two blending runs were regarded as outliners due to its dramatic trend difference compared to its replicates. The remaining 22 runs were used for further data analysis.

2.4.1.1.2. Root mean square from nominal value (RMSNV). Predicted and nominal concentrations were used to calculate root mean square from nominal value for each blending experiment according to the following equation:

$$\mathrm{RMSNV} = \sqrt{\frac{(P_{\mathrm{APAP}} - N_{\mathrm{APAP}})^2 + (P_{\mathrm{LAC}} - N_{\mathrm{LAC}})^2 + (P_{\mathrm{MCC}} - N_{\mathrm{MCC}})^2}{3}} \quad (1)$$

where P is the predicted concentration for each component at a single sensor position and N is the nominal concentration for each component.

2.4.1.1.3. Student's t-test. A Student's t-test (two-tailed) was performed between every 12 RMSNV points (1 min interval) and zero. Confidence interval (CI, 95%) was calculated and plotted with respect to time. The end-point was regarded as the time-point at which the upper CI deviates less than 12% from nominal, and the lower CI deviates less than 2% from nominal.

2.4.1.2. End-point determined by API predicted concentration profile. The same NIPLS model as 2.4.1.1.1 was established to predict API concentrations. After API concentrations were plotted against time, relative standard deviation (R.S.D.) of every three continuously predicted concentrations was calculated. Due to the high rate of spectra collection, another window of nine was used to smooth the trend of R.S.D. The end-point was reached when R.S.D. was smaller than 5%, according to FDA guidance on blending [22].

2.4.1.3. End-point determined by moving-window standard deviation. Spectra were preprocessed by standard normal variate before end-point determination. Based on previous algorithms [5–7], the standard deviation (S.D.) at an individual wavelength was calculated using a window of three consecutive spectra; mean value of S.D. across the whole wavelength range was then calculated to represent the spectral variation within the time window; each successive value was determined by shifting the window (in time) by one sample until all acquired spectra were utilized. Due to the high rate of spectra collection, another window of nine was used to smooth the trend of mean S.D. The first zero-crossing point of the first derivative of the smoothed mean S.D. trend was regarded as the end-point of mixing.

2.4.2. The effect of model performance on end-point determination

Due to the better performances of top sensor, only data collected from the top sensor were used here. The effect of model performance parameters on end-point determination was investigated by adjusting the number of PCs, slope and bias deviation of prediction. Slope and bias deviation of ±20%, ±10% and ±5% were performed.

2.4.3. End-point determination and blending variability characterization by two sensors

The similar end-point determination protocol was performed except for the following modifications. Due to the discrepancy of measurement error on different blending runs by different sensors, RMSNV was rescaled by subtracting individual pure error for each blending run by each sensor. Measurement error was calculated using the following equation:

$$\mathrm{PE} = \sqrt{\frac{\sum_{i=1}^{200}(C_{\mathrm{API}} - \bar{C}_{\mathrm{API}})^2 + \sum_{i=1}^{200}(C_{\mathrm{LAC}} - \bar{C}_{\mathrm{LAC}})^2 + \sum_{i=1}^{200}(C_{\mathrm{MCC}} - \bar{C}_{\mathrm{MCC}})^2}{200 \times 3}} \quad (2)$$

where PE is the pure error of concentration prediction on single blending run by single sensor, C the individual predicted concentration among the last 200 spectra at the end of blending process and $\bar{C}$ is the mean predicted concentration of last 200 spectra at the end of blending process.

After pure error of each sensor on each blending run was removed, a Student's *t*-test (two-tailed) was performed as before followed by calculation of 95% CI. Due to the subtraction of pure error from RMSNV, RMSNV at certain time points showed negative values. Thus, the end-point determination criteria was modifies as follows: for the top sensor, end-point was determined as the point at which the upper and lower CIs deviated less than 5 and −5% from nominal, respectively. For the side sensor, the end-point was determined to be the point at which the upper and lower CIs deviated less than 15 and −5% from nominal, respectively. After end-point was measured, 120 RMSNV points (10 min interval) after end-point were chosen to calculate the mean and standard deviation, representing the blending variability at the end-point.

3. Results and discussion

Partial least squares (PLS) is a mathematical method that is capable of describing the covariance between multidimensional NIR spectral data and response variables by means of a small number of non-intercorrelated variables or principal components. Non-linear iterative partial least squares is a standard algorithm for computing PLS regression components, which can be used for both univariate and multivariate Y data. The information of NIPLS models for top sensor was as follows: four principle components, 97.65% of X and 93.97% of Y variance were captured. Savitzky–Golay smoothing and second derivative (SG) was chosen as a preprocessing technique to correct the baseline of spectra. The baseline correction is expected to suppress physical interference and therefore enhance chemical information. The advantages of using SG was demonstrated by the lower RMSEC and RMSECV using smaller number of principle components compared to other preprocessing techniques in Table 2. The spectral similarity between regression vectors and pure components indicated the specificity of PLS model on capturing concentration variation of individual component (Fig. 2).

A representative PLS predicted concentration plot during a blending run is shown in Fig. 3. It was observed that a longer blending time was required for LAC and MCC to reach their target values compared to APAP. It is well understood that the physical and chemical properties of blend constituents substantially affect the time

Table 2
Calibration statistics for NIPLS model

	PCs	RMSEC (%, w/w)	RMSECV (%, w/w)
SG	4	2.82	3.09
SNV	4	4.10	4.76
	5	2.69	3.08
Detrend	5	4.34	5.08

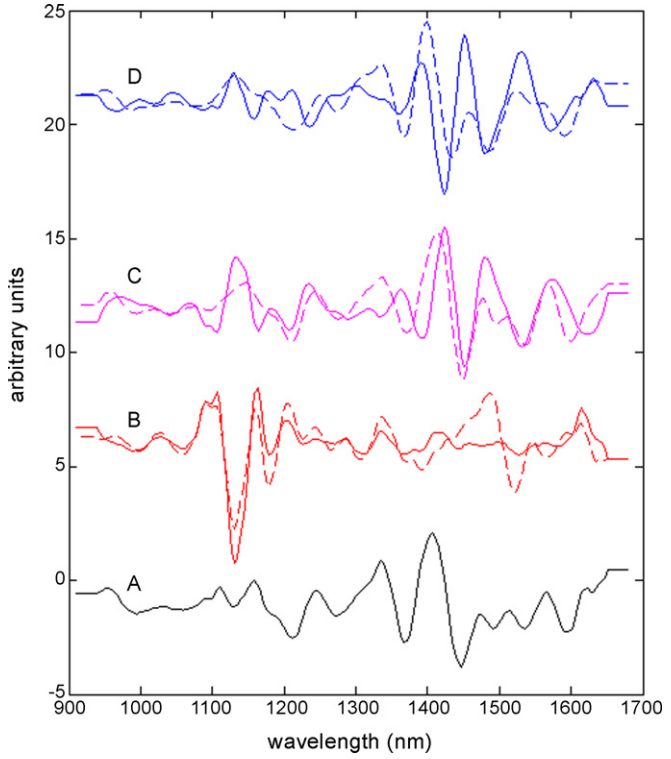

Fig. 2. Comparison among regression vectors, pure component spectra and example spectra collected at the end of blending process. (A) Preprocessed spectra collected at the end of blending process. (B–D) Regression vectors and preprocessed pure component spectra for APAP, LAC and MCC. Solid lines represented the regression vectors, dotted lines represented pure component spectra after second-derivative pre-treatment.

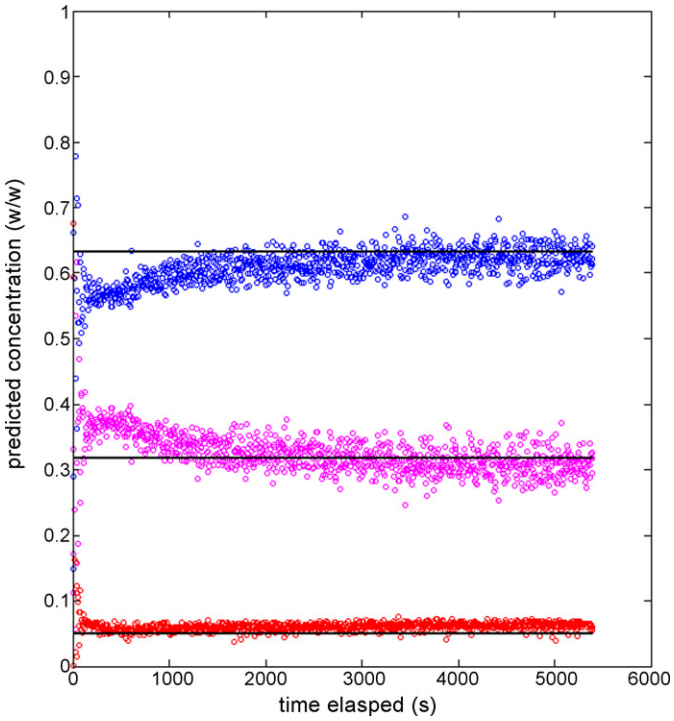

Fig. 3. Example predicted concentration plot for a representative run based on the top sensor. The nominal value for each component (w/w) was as follows: MCC (63.3%, top), lactose (31.7%, middle) and APAP (5%, bottom). The solid lines represent the nominal values for each component.

required to distribute these components throughout a blend. In this particular example, the model API was distributed relatively quickly, while the excipients required a longer time to reach the target concentrations. This specific example highlights the necessity of monitoring not only API, but excipients as well. A blend such as this would have been considered homogenous prior to the final mixing of the excipients if only the API were monitored. If such a blend were allowed to proceed through subsequent pharmaceutical unit operations, a substantial variability would be introduced to the resulting finished product.

Concentration prediction for individual constituents at the end of blending process had different variances. These fluctuations were observed when the target concentration was reached (Fig. 3). Variance observed can be attributed to two factors. First, prediction errors contributed to the variability (the reason for removing pure error when two sensors were compared later). Second, more importantly, variability in constituent concentration at the sensing window should be expected to occur and is expected to explain a significant portion of the observed fluctuations. The inherent variability of the blending process is the driving force for applying the Student's *t*-test to RMSNV calculations; as, the Student's *t*-test takes into account of absolute deviation between current and target concentrations and variance of current blending profile.

The concentration profiles from the PLS predictions directly represent the concentration of materials at the sampling point through time. An estimated end-point can be determined by observation of these results. However, a more robust metric is necessary for in-line process monitoring in order to determine end-point mathematically and stop blending rotation automatically. An ideal method would include sensitivity to target concentrations for the blend, characteristic concentration variability at end-point, continuity of measurements and predicted blend status immediately following blend end-point. Further, the metric must express these characteristics in a single value. A sensitivity to target concentrations assures that the blend has achieved not just self-consistency, but an agreement with the required level of each constituent. Constituent variability at the end-point should be relatively consistent from blend to blend. A lack of consistency among blends as measured by the blend variability at the end-point is indicative of changes in the properties of the materials. The requirement of consistency after blend end-point is meant to assure that a blend will not oscillate between "blended" and "non-blended" after the blend end-point. Such oscillations should not be an artifact of the calculation; rather, they should be a function of constituent properties.

The metric selected to meet the criteria of agreement with target concentration and a single value representing all blend concentrations was root mean square from nominal value (Eq. (1)). This metric summarizes the difference between each predicted concentration and its target value for all the components. A representative RMSNV plot is shown in Fig. 4; in this figure it is observed that a large RMSNV at early time points indicating inhomogeneous mixture. As time elapsed and blending continued, RMSNV decreased until it reached a plateau. A 95% CI was calculated based upon the last 12 points to illustrate the rate of change of variability. Due to the heterogeneity at initial blending process, 95% CIs were far away from the threshold limit. With time, both CIs converged within 2–12% deviation from nominal, indicating that the blending process had reached a desired degree of homogeneity (from a statistical standpoint).

In the study, equal weight was used for each component when RMSNV was calculated in order to illustrate the importance of monitoring blending process based on all the constituents (Eq. (1)). In practical use of RMSNV, the relative weight of each component may be determined based upon manufacturing and regulatory requirements (Eq. (3)). For instance, the weights of excipients are expected

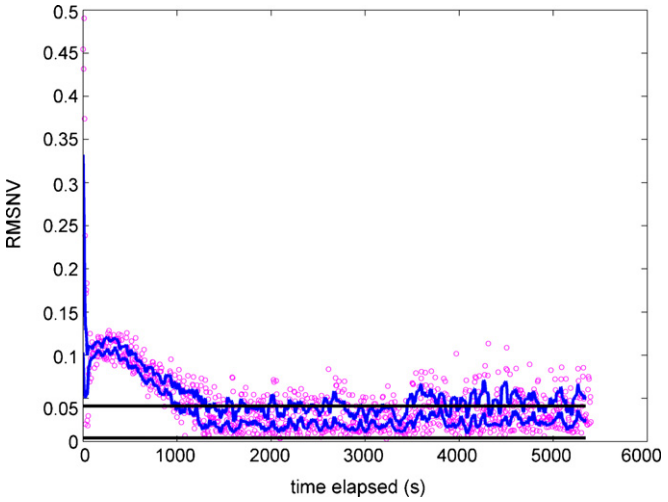

Fig. 4. Example for RMSNV plot for certain a blending experiment. Dots represented RMSNV at each sampling point. Solid curves represented 95% CI. Solid lines represented 2% and 12% deviation from nominal value.

to increase when the excipients are designed to play significant roles controlling the *in vitro* and *in vivo* drug release. In that case, monitoring powder blending process can become initiative to control drug release profile. Another example is to add more weight to API (increase W_{API}) to account for low-dose formulations in order to monitor strictly API blending profiles. Thus, the RMSNV calculation allows freedom to adjust process control strategies via the weight according to different requirements of the manufacturing process and final dosage form.

$$\text{RMSNV}=\sqrt{\frac{W_{APAP}(P_{APAP}-N_{APAP})^2+W_{LAC}(P_{LAC}-N_{LAC})^2+W_{MCC}(P_{MCC}-N_{MCC})^2}{W_{APAP}+W_{LAC}+W_{MCC}}} \quad (3)$$

where W is the relative weight of constituents.

Monitoring the collapse of the CI to the 2–12% deviation level is equivalent to performing a Student's *t*-test. The advantage of a Student's *t*-test is that it captures the end-point based on mean value (closeness to zero) and variance at the inflection point of RMSNV

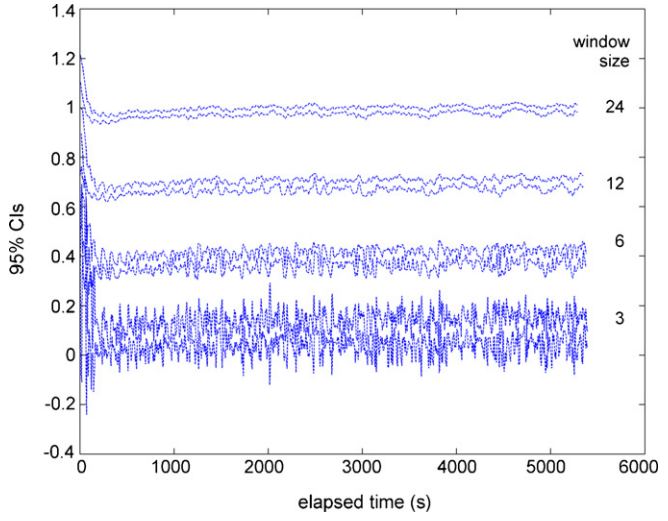

Fig. 5. The effect of window size selection on 95% CIs. The plots from the top to the bottom represented the results using window size of 24, 12, 6 and 3 on a representative blending run. The upper three plots were offset for clarity.

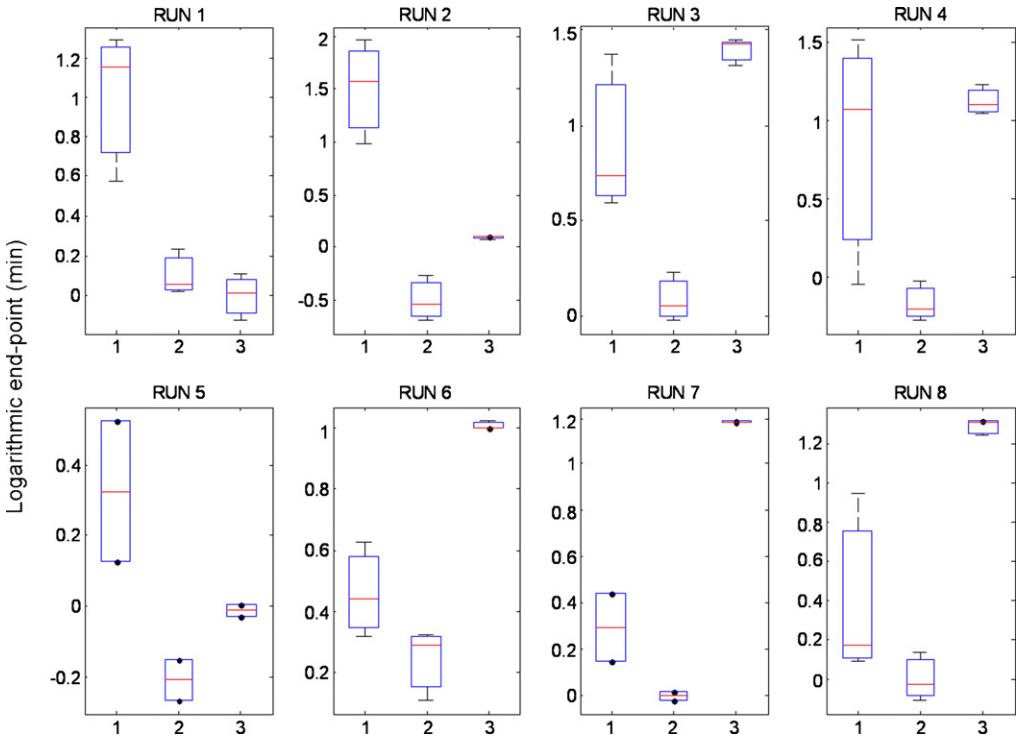

Fig. 6. Comparison of robustness of different end-point determination algorithms. (1) API prediction profile. (2) Moving-window standard deviation. (3) The multivariate model-based approach. *Y*-Axis was logarithmic transformed in order to highlight the difference of variance of end-point among replicates determined by different end-point determination algorithms. The lines in the boxes are at the lower quartile, median, and upper quartile values. The whiskers are lines extending from each end of the boxes to show the extent of the rest of the data.

profile of the blend. While it has been suggested that *P* or *T* values would serve as a suitable metric to determine end-point, confidence intervals have been observed to be more robust in end-point determination in cases where blending variability at the end-point was either comparatively small or large.

The threshold limit (2–12%) was selected based on the observed blending process variation within the current design matrix. The threshold limit may be restricted to a smaller range to require a closer agreement of the target levels and variability under different circumstances. However, the current system included a wide variety of target constituent levels and properties necessitating a wider threshold for end-point determination.

The number of RMSNV points included in the window for calculation of CIs can affect the end-point determination. The window should be as small as possible to allow a rapid response to process changes and yet, of adequate duration to obtain a representative sample. A window size of twelve was utilized to perform the calculation. Fig. 5 illustrates the effect on CIs of changing window size. Note that as the window size is increased the effective CI is decreased; however, at window sizes greater than 12, the decrease in CI is nominal. Thus, this was the smallest window that demonstrated adequate sensitivity for end-point determination. For reference algorithms, three as window size was used to calculate spectral standard deviation for MVSD and relative standard deviation for API predicted concentration. However, it was necessary to smooth the results and a nine-point window was used for that purpose. Thus, the total number of points for a given prediction was 12 for both the reference and the proposed algorithm.

The proposed algorithm was compared to the reference algorithms to assess stability of end-point determination and suitability for use in the current system. Compared to end-point determined by MVSD and API predicted concentration profile, the multivariate model-based algorithm consistently demonstrated the lowest variance of end-point determination among replicates across the whole design matrix (Fig. 6). This indicates the improved robustness of the multivariate method compared to other widely employed end-point determination algorithms.

The enhanced robustness is attributed to the following properties of the multivariate model-based approach. First, the specificity of multivariate model enhanced the capacity to capture individual concentration variation, particularly in the case of spectrally similar components such as LAC and MCC. It was observed from pure component spectra that LAC was similar to MCC (Fig. 7). Since LAC

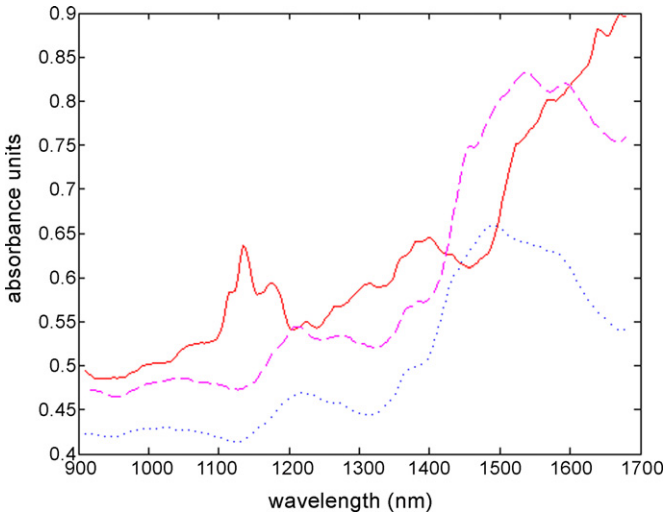

Fig. 7. Pure component spectra. Solid line (APAP); dashed line (LAC); dotted line (MCC).

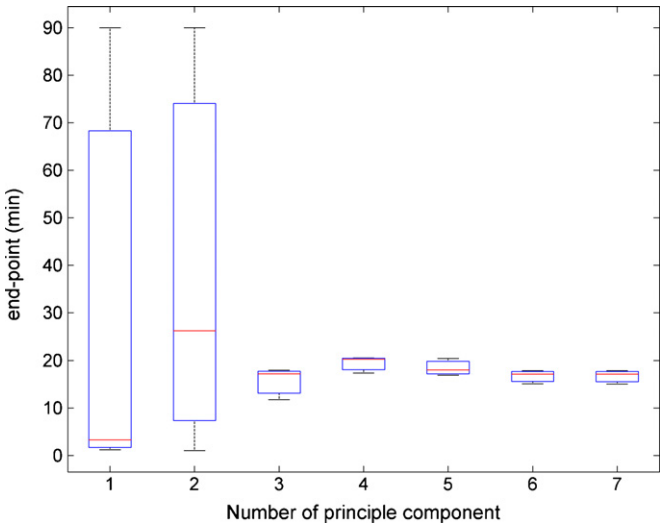

Fig. 8. Effect of the number of principle component on observed end-point determination.

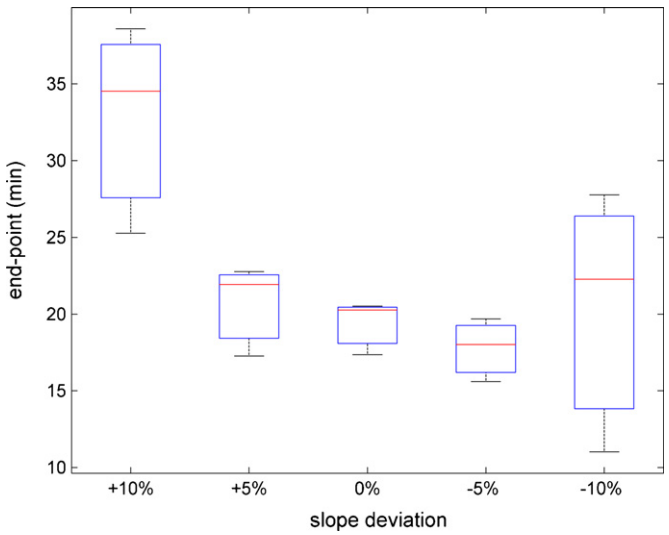

Fig. 10. Effect of slope deviation of prediction on observed end-point determination.

and MCC were the major constituents in the blending composition, the MVSD was only sensitive to the variation of APAP due to its unique spectral features compared to LAC and MCC. Thus, it was not possible for MVSD to capture blending variation of LAC and MCC. Although spectral preprocessing was able to enhance spectral features of individual constituents at specific wavelengths, the mean value of standard deviation across the wavelength range removed the enhanced spectral difference at specific wavelengths. Second, the MVSD generated a noisier signal across the wavelength range compared to the multivariate model-based approach. Since the approach was calibrated against concentration variation, specific wavelength regions corresponding to chemical information was enhanced in the regression vector, while noise-related wavelength regions were suppressed.

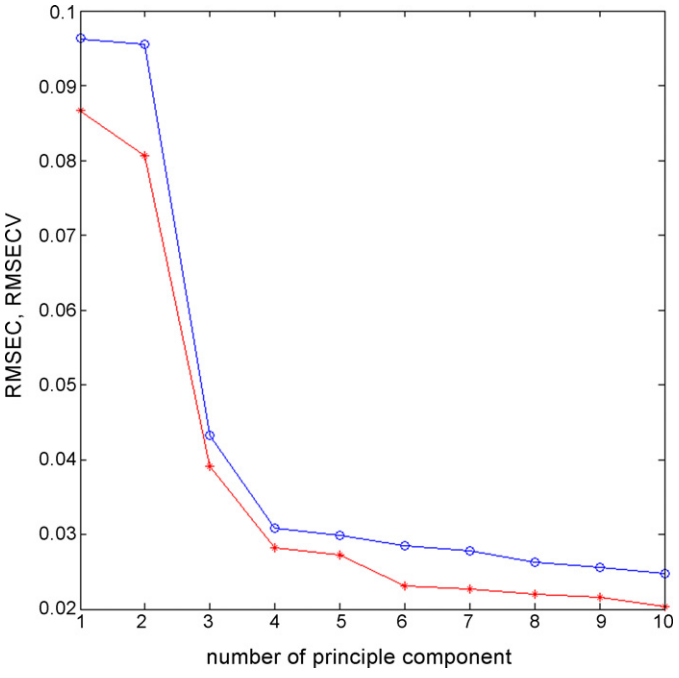

Fig. 9. Effect of the number of principle component on RMSEC and RMSECV for NIPLS calibration. Asterisk represented RMSEC, circle represented RMSECV.

Blend design point #8 was selected to demonstrate the effect of model performance on end-point determination. Other blending design points demonstrated similar trends (data not shown). It is demonstrated in Fig. 8 that the variance of end-point determination was dramatically decrease when more than two PCs were used. Further, using one or two PCs caused the system to be under-modeled. This trend was further confirmed in the difference of RMSEC and RMSECV using only first two PCs compared to that using three or more PCs (Fig. 9). Data from other blend design points indicate that the use of an additional PC (total of four PCs) enhanced the ability to capture concentration variation in the system. The additional PC was required to account for the variance of each blending run in the multi-dimensional space.

The effects of slope and bias deviations on blend end-point determination were investigated. Figs. 10 and 11 demonstrate that both slope and bias deviations increased the variance of end-point determination, indicating that careful supervision of both slope and bias is necessary in order to maintain the routine model performance. Slope deviation confirmed a more asymmetric effect on end-point determination compared to bias deviation. It can be attributed to the following. In the current design matrix, LAC and

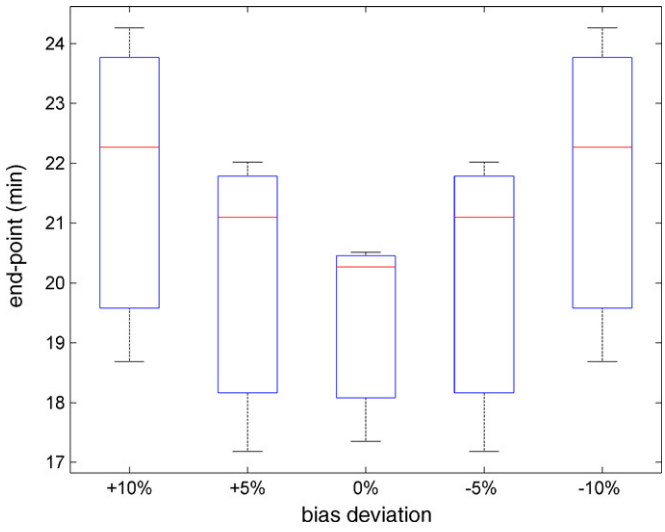

Fig. 11. Effect of bias deviation of prediction on observed end-point determination.

MCC were observed to show inverse predicted concentration trend with respect to time (e.g. Fig. 3). Since bias deviation gave each constituent the same amount of deviation, possible bias deviation of LAC can be offset by that of MCC. However, the slope deviation was greater for the constituent with large predicted concentration compared to the component with small predicted concentration; thus, the blending end-point was likely driven by the constituent of large predicted concentration. Additionally, a probability function was calculated to characterize the stability after end-point was reached; the number of RMSNV points within threshold limit after end-point was divided by the total 120 RMSNV points (10 min interval). A good blending run should reach the end-point as quickly as possible and possess consistent stability after end-point, with stability probability value close to unity. As deviations were increased to 10%, stability probability function decreased to a value smaller than 0.5 despite the fact that the blend was not changing. This deviation caused, in effect, a false-positive test for demixing after end-point was reached. Upon increasing the slope and bias deviation to 20%, no end-point was detected. Although stability probability function required data after end-point to determine the stability of a blending process, it could become one of promising metrics to study and characterize blending variability at end-point during research and development in order to select the "target" blending operation with the optimal blending stability.

Performances of the top and side sensors were compared for characterization of end-point and blending variability. RMSNVs were corrected for measurement errors of each sensor on each blending run by subtracting pure error from RMSNV. First, it was observed in pair-wised *t*-test that the pure error determined by side sensor was significantly larger than that of top sensor ($P = 0.0109$, 95% CI was 0.0011–0.0072). This can be attributed to the intrinsic properties of two spectrometers. Compared to the side sensor, the top sensor had a stronger light source, a higher signal to noise ratio and a larger interrogation volume. Second, a one-way ANOVA demonstrated that certain blending design points had significantly larger pure error compared to other designs ($P = 1.7 \times 10^{-5}$ for side sensor, $P = 2.1 \times 10^{-5}$ for top sensor). Thus, individual pure error for each blending run determined by each sensor was utilized to remove the measurement error from RMSNVs before the *t*-test in order to capture the original RMSNV information from the blending processes.

After rescaling RMSNV, end-point determinations by the two sensors were compared. A pair-wise *t*-test demonstrated that end-points detected by top sensor were significantly longer than that by side sensor ($P = 0.0011$, 95% CI was 3.4080–11.7360 min). Subsequently, mean and standard deviation of RMSNV at the end-point were used to characterize the blending variability determined by the two sensors. The pair-wise *t*-test additionally demonstrated that both mean and standard deviation of RMSNV from top sensor were significantly smaller than those from side sensor, which also supported the smaller threshold limit for top sensor (−5 to 5%) compared to side sensor (−5 to 15%) as criteria to determine end-points. The statistics were as follows: $P = 1.6 \times 10^{-7}$ and 95% CI was −0.0243 to −0.0140 for mean RMSNV, $P = 9.8 \times 10^{-8}$ and 95% CI was −0.0096 to −0.0056 for standard deviation of RMSNV. Considering the difference of end-point determination and variability characterization by two sensors, it indicated that blending behavior at top surface differed significantly from the side wall of the Bin-blender, requiring more time and reaching end-point with smaller variability. The causal factors for different blending behaviors at different locations are currently under investigation. It is difficult to conclude that one sensor location is better than the other since only two sensor locations were studied. But the results were similar to the paper published by Wightman et al., in which the mixing patterns at internal cross-sections were demonstrated to differ significantly from patterns observed at end walls [23]. Thus, it can be concluded that observations at one blending location may not be representative of the total powder blending processes inside the Bin-blender. This clearly demonstrates the advantage of employing process monitoring by NIR spectroscopy at more than one location in order to capture the blending variance sufficiently.

4. Conclusion

The algorithm of employing multivariate models to predict constituent concentrations followed by RMSNV and two-tailed *t*-test is a promising metric for monitoring powder blending. Use of customized weighting factor in the metric allows different process control strategies according to performance requirements of manufacturing process and final solid dosage form. Compared to widely employed end-point determination algorithms, the multivariate model-based algorithm demonstrated more robustness for end-point determination by accounting for both constituent concentrations and variances.

The use of two differently located sensors demonstrated different blending behaviors, including greater blending variability at side wall and longer blending time at top surface. This study indicates the superiority of monitoring powder blending via NIR spectroscopy at more than one location on the Bin-blender in order to capture overall blending variation.

References

[1] G. Reich, Adv. Drug Deliv. Rev. 57 (2005) 1109–1143.
[2] R.P. Cogdill, J.K. Drennen, in: H. Brittain (Ed.), Near-Infrared Spectroscopy, in Spectroscopy of Pharmaceutical Solids, Taylor & Francis, New York, 2006, pp. 313–412.
[3] F.C. Sanchez, J. Toft, B. van der Bogaert, D.L. Massart, S.S. Dive, P. Hailey, Fresenius J. Anal. Chem. 352 (1995) 771–778.
[4] M. Blanco, R.G. Bano, E. Bertran, Talanta 56 (2002) 203–212.
[5] S.S. Sekulic, H.W. Ward, D.R. Brannegan, E.D. Stanley, C.L. Evans, S.T. Sciavolino, P.A. Hailey, P.K. Aldridge, Anal. Chem. 68 (1996) 509–513.
[6] S.S. Sekulic, J. Wakeman, P. Doherty, P.A. Hailey, J. Pharm. Biomed. Anal. 17 (1998) 1285–1309.
[7] A.S. El-Hagrasy, H.R. Morris, F. D'Amico, R.A. Lodder, J.K. Drennen 3rd, J. Pharm. Sci. 90 (2001) 1298–1307.
[8] R. De Maesschalck, F.C. Sanchez, D.L. Massart, P. Doherty, P. Hailey, Appl. Spectrosc. 52 (1998) 725–731.
[9] A.S. El-Hagrasy, M. Delgado-Lopez, J.K. Drennen, J. Pharm. Sci. 95 (2006) 407–421.
[10] D.J. Wargo, J.K. Drennen, J. Pharm. Biomed. Anal. 14 (1996) 1415–1423.
[11] O. Berntsson, L.G. Danielsson, B. Lagerholm, S. Folestad, Powder Technol. 123 (2002) 185–193.
[12] M. Popo, S. Romero-Torres, C. Conde, R.J. Romañach, AAPS PharmSciTech. 3 (2002) (article 24).
[13] N.H. Duong, P. Arratia, F. Muzzio, A. Lange, J. Timmermans, S.A. Reynolds, Drug Dev. Ind. Pharm. 29 (2003) 679–687.
[14] R.L. Green, M.D. Mowery, J.A. Good, J.P. Higgins, S.M. Arrivo, K. McColough, A. Mateos, R.A. Reed, Appl. Spectrosc. 59 (2005) 340–347.
[15] W. Li, M.C. Johnson, R. Bruce, S. Ulrich, H. Rasmussen, G.D. Worosila, Int. J. Pharm. 326 (2006) 182–185.
[16] E.T.S. Skibsted, H.F.M. Boelens, J.A. Westerhuis, D.T. Witte, A.K. Smilde, J. Pharm. Biomed. Anal. 41 (2006) 26–35.
[17] A.S. El-Hagrasy, J.K. Drennen, J. Pharm. Sci. 95 (2006) 422–434.
[18] V. Swaminathan, D.O. Kildsig, Drug Dev. Ind. Pharm. 28 (2002) 41–48.
[19] O.S. Sudah, D. Coffin-Beach, F.J. Muzzio, Powder Technol. 126 (2002) 191–200.
[20] F.C. Clarke, S.V. Hammond, R.D. Jee, A.C. Moffat, Appl. Spectrosc. 56 (2002) 1475–1483.
[21] J.H. Cho, P.J. Gemperline, P.K. Aldridge, S.S. Sekulic, Anal. Chim. Acta 348 (1997) 303–310.
[22] Guidance for Industry, Powder Blends and Finished Dosage Units—Stratified In-Process Dosage Unit Sampling and Assessment, http://www.fda.gov/CDER/GUIDANCE/5831dft.htm.
[23] C. Wightman, P.R. Mort, F.J. Muzzio, R.E. Riman, E.K. Gleason, Powder Technol. 84 (1995) 231–240.